

Produced water re-injection in a non-fresh water aquifer with geochemical reaction, hydrodynamic molecular dispersion and adsorption kinetics controlling: model development and numerical simulation

Ibidapo Obe¹ · T. A. Fashanu¹ · Peter O. Idialu¹ · Tope O. Akintola² · Kingsley E. Abhulimen²

Received: 20 October 2013 / Accepted: 11 October 2016 / Published online: 27 December 2016
© The Author(s) 2016. This article is published with open access at Springerlink.com

Abstract An improved produced water reinjection (PWRI) model that incorporates filtration, geochemical reaction, molecular transport, and mass adsorption kinetics was developed to predict cake deposition and injectivity performance in hydrocarbon aquifers in Nigeria oil fields. Thus, the improved PWRI model considered contributions of geochemical reaction, adsorption kinetics, and hydrodynamic molecular dispersion mechanism to alter the injectivity and deposition of suspended solids on aquifer wall resulting in cake formation in pores during PWRI and transport of active constituents in hydrocarbon reservoirs. The injectivity decline and cake deposition for specific case studies of hydrocarbon aquifers in Nigeria oil fields were characterized with respect to its well geometry, lithology, and calibrations data and simulated in COMSOL multi-physics software environment. The PWRI model was validated by comparisons to assessments of previous field studies based on data and results supplied by operator and regulator. The results of simulation showed that PWRI performance was altered because of temporal variations and declinations of permeability, injectivity, and cake precipitation, which were observed to be dependent on active adsorption and geochemical reaction kinetics coupled with filtration scheme and molecular dispersion. From the observed results and findings, transition time t_r to cake nucleation and growth were dependent on aquifer constituents, well capacity, filtration coefficients, particle-to-

grain size ratio, water quality, and more importantly, particle-to-grain adsorption kinetics. Thus, the results showed that injectivity decline and permeability damage were direct contributions of geochemical reaction, hydrodynamic molecular diffusion, and adsorption kinetics to the internal filtration mechanism, which are largely dependent on the initial conditions of concentration of active constituents of produced water and aquifer capacity.

Keywords Reinjection · PWRI · Cake formation · Aquifer · Adsorption kinetics · Produced water

List of Symbols

S_T	Skin factor
μ	Viscosity
P_{inj}	Injection pressure
q	Flow rate (m^3/s)
k	Permeability
k_σ	Permeability damage factor
η	Total collision probability
η_l	Collision probability due to interception
η_D	Collision probability due to diffusion
η_{lm}	Collision probability due to impaction
η_s	Collision probability due to sedimentation
η_E	Collision probability due to surface forces
d_p	Particle diameter
d_g	Grain diameter
ϕ	Effective porosity
ρ_p	Particle density
ρ_f	Fluid density
U, u	Darcy's velocity
g	Gravity acceleration (m/s^2)
T	Absolute temperature K ($^\circ C$)
$C(r, t)$	Volumetric concentrations of suspended particles, ppm

✉ Kingsley E. Abhulimen
syntechsystworld@gmail.com

¹ Department of Systems Engineering, University of Lagos, Lagos, NG, Nigeria

² Department of Chemical and Petroleum Engineering, University of Lagos, Lagos, NG, Nigeria

$\sigma(r, t)$	Volumetric concentrations of the deposited particles, ppm	Produced water constituents	Heavy metals, suspended solids, dissolved solids, hydrocarbon traces, etc.
k_o	Absolute permeability		
λ	Filtration coefficient	Injection pipe	Produced water transfer medium from surface to sub-surface
L	Depth of the porous media		
ε_r	Scaled length in radial direction	Well bore	Point of contact of injection pipe with formation/reservoir
ε_z	Scaled length in axial direction		
t	Time (years)	Deep bed filtration	The flow and deposition of particles in the rock matrix
τ	Scaled time		
\in	Scaled concentration of suspended solids	Injectivity decline	Index signifying the change in the injection rate of the injected fluid
S	Scaled concentration of deposited particles		
λ_o	Initial filtration coefficient	Formation damage	Reduction in aquifer properties that are solely responsible for the transmissibility of reservoir fluids through the pore spaces (fracture in internal walls of the aquifer)
α_c	Clean bed collision efficiency		
I	Injectivity index		
J	Inverse of injectivity index		
T_r	Transition time		
N	Number of particles attached to one grain	Adsorption kinetics	Attraction and retention of particle to the surface grain and the preference of this particle for a particular site within the reservoir
J_d	Impedance during one-phase suspension flow		
K_{ror}	Relative permeability of residual oil		
m	Slope of impedance straight line during deep bed filtration for one-phase suspension flow	Hydrodynamic dispersion	Is a term used to include both diffusion and dispersion of particles within a medium
m_c	Slope of impedance straight line during external cake formation for one-phase suspension flow		
p	Pressure (M/LT ² Pa)	Geochemical reaction	This is the interaction of species constituents in the produced water and the formation of the host aquifer
q	Total flow rate per unit reservoir thickness (L ² /T)		
r	Reservoir radius (L, m)		
r_w	Well radius (L/m)		
r_d	Damage zone radius (L, m)	Colloids	Colloidal particles are suspended particles carried in the fluid stream
R_c	Contour radius (L/m)		
S_{or}	Residual oil saturation	Scales	Result of nucleation of colloids
S_{wi}	Initial water saturation	Cakes	Deposition of scales in pore sites is referred to as cakes
T	Time (T, s)		
T	Dimensionless time	Geomechanics	Involves the geologic study of the behaviour of soil and rock
T_{tr}	Dimensionless transition time		
U	Total flow velocity (L/T, m/s)	Corrosion	Loss in metal due to degradation, erosion or prevailing ambient conditions
α	Critical porosity fraction		
β	Formation damage coefficient		
ϕ	Porosity	Souring	Acidic smell/taste characteristic

Definition of terms and acronyms

Produced water	Water associated with crude oil exploration and production	Elementary volume	A pictured or drawn shape representative of the actual shape. Used in solving mathematical problems
Produced water re-injection	Sending back produced water from the surface into the sub-surface	Isotherms	Equations considered at constant temperature
Non-fresh water hydrocarbon aquifer	Crude oil bearing formation	Finite-element method	Numerical method of solution whereby a problem is characterized by boundaries and solved within these boundaries
Reservoir	A permeable subsurface rock that contains petroleum	PW	Produced water
Formation	Refers to the reservoir bearing fluids, e.g., oil, gas, and water	PWRI	Produced water re-injection
		EOR	Enhanced oil recovery

E & P	Exploration and production
REV	Representative elementary volume
TVD	Total vertical depth
BHP	Bottom hole pressure

Introduction

Reinjection of produced water into spent hydrocarbon aquifer also referred to as produced water reinjection (PWRI) is one of the earliest and most environment friendly methods to dispose produced water from production platforms. However, reinjection of produced water degrades the aquifer that results in injectivity decline, fracturing of the internal walls of the aquifer and later formation damage, as shown in Fig. 1. Thus, PWRI has reduced performance over a period, because the method cannot be sustained throughout the production life of the reservoir.

Previous studies and models described processes and mechanisms that resulted in formation damage and cake formation which were well developed and documented in technical literatures. PWRI in aquifers is generally studied under two research domains: (1) internal filtration and (2) external cake build up (Bedrikovetsky et al. 2001; Bedrikovetsky et al. 2007; Wennberg and Sharma 1997; Farajzadeh 2002; Al-Abduwani 2005). Significant research works and models were advanced and documented in several technical literatures to predict injectivity and characterize formation damage system and well behavior (Pang and Sharma 1994, 1997; Ojukwu and van den Hoek 2004; Guedes et al. 2006; Yerramilli et al. 2013).

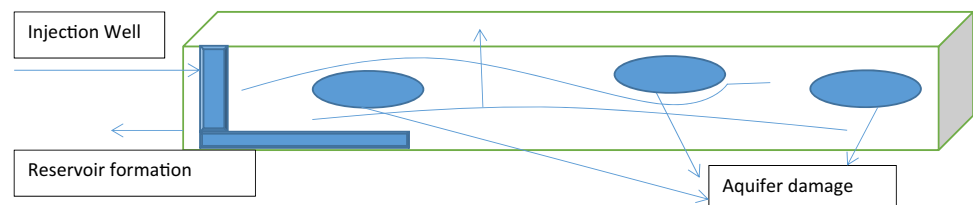
Precious studies show that formation damage and injectivity decline are two major drawbacks associated with PWRI performance in hydrocarbon aquifer. Some past and recent studies were focused on understanding formation damage mechanisms (Salehi and Settari 2008; Prasad et al. 1999; Davidson 1979; Marchesin et al. 2011; Abou-Sayed et al. 2005; Zhang et al. 1993; Todd 1979; Ochi et al. 2007; Nabzar et al. 1997; De Zwart 2007; Faruk 2010; Lawal et al. 2011; Lawal and Vesovic 2010; Wang and Le 2008; Li et al. 2012).

There are other studies and models available in technical literature targeted to predict injectivity decline from par-

ticulate mechanics and flow transport. Notable contributions in this regard include work of Barkman and Davidson (1972), Pang and Sharma (1994, 1997) as well as Wennberg and Sharma (1997). In theory, efficiency and sustainability of the PWRI were progressed by considering injectivity decline as an outcome of momentum and particulate transport phenomena in porous media (Mendez 1999). There are other model and studies reported in technical literatures by previous researchers that focused on the filtration coefficient as the sole determinant of injectivity decline and fracturing (Abou-Sayed et al. 2007; Ajay and Sharman 2007, Al-Abduwani et al. 2001; Altoef et al. 2004; Chang 1985; Clifford et al. 1991; Donaldson et al. 1977; Doresa et al. 2012; Folarin et al. 2013; Gong et al. 2013; Hustedt et al. 2006). None of these models hinted on possible geochemical reaction of produced water heavy metals and aquifer water constituents and effect of geochemical reaction, the focus of this research study.

Nevertheless, recent findings (Idialu 2014) suggest a significant role of adsorption, geochemical reaction and molecular transport kinetics in well behavior, cake formation and damage characterization in PWRI modeling, and field data analysis. Therefore, this paper considers the effects of geochemical reaction, adsorption kinetics, and hydrodynamic molecular transport in formation damage and injectivity decline modeling and developments. Performance of PWRI water injectivity decline as a function of injection water quality, rates, and pressures was found to be significant factors in well injection design and formulation of secondary and tertiary recovery strategies. The effect of geochemical reaction in scale formation to injectivity decline was considered in the PWRI model analysis while outlining also the role of adsorption kinetics and molecular transport. The justification of this work inspired by the significant and active research interest over the last decade in the use of produced water as a resource in reinjection as alternative secondary and tertiary recovery method could achieve the goals of the zero tolerance by regulatory authority to water disposal management to maintain marine life and environment sustainability.

Fig. 1 Collapsed features where fracture will be more prevalent



Model development

The aquifer grid for produced water system and geometry of the PWRI schemes in well-reservoir formation, effects, and problems encountered were illustrated in Figs. 2 and 3, respectively. The implications arising from PWRI management are: (1) injectivity loss; (2) permeability loss; (3)

loss of recovery; (4) loss in reservoir potential; (5) poor reservoir sweep (bypass oil and early water breakthrough); (6) excessive chemical treatment; and (7) discharge not meeting environmental regulations.

The generalized improved PWRI model incorporated molecular transport, geochemical, and adsorption kinetics in Eq. 1 with boundary conditions presented in Eqs. 2, 3, and 4:

Fig. 2 Generic aquifer grid system for produced water re-injection system. C_{in} Concentration of active constituents in produced water in Reservoir-Aquifer Control volume grid, C_{out} Concentration of active constituents in produced water out Reservoir-Aquifer Control volume grid. $U_x in, U_y in, U_z in$ is the velocity of produced water in Cartesian coordinates x, y, z in Reservoir-Aquifer Control volume grid. $U_{xout}, U_{yout}, U_{zout}$ is the velocity of produced water in Cartesian coordinates x, y, z out Reservoir-Aquifer Control volume grid

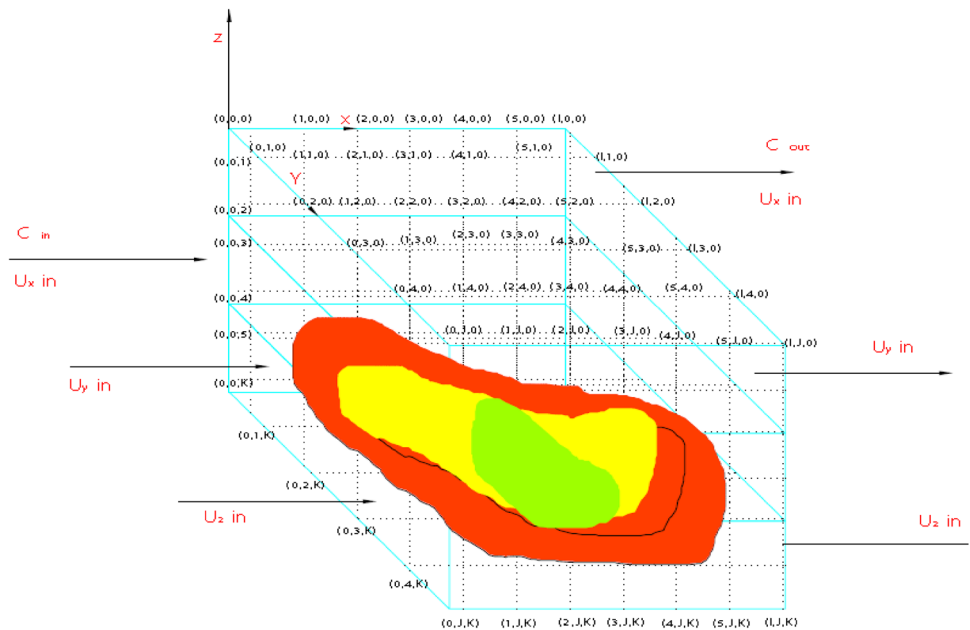
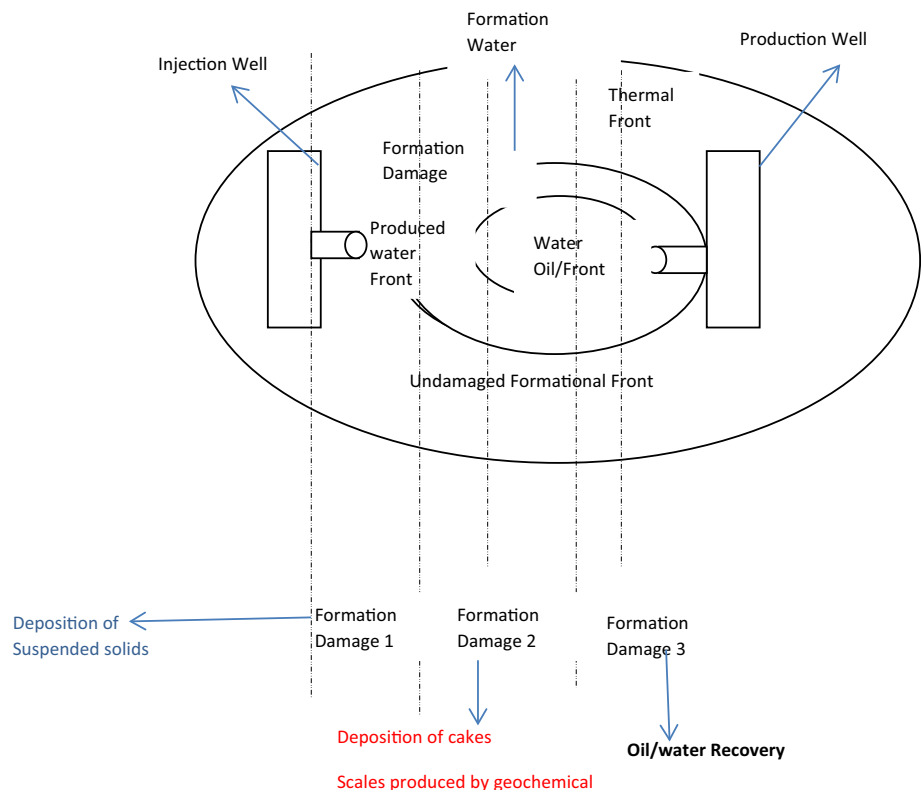


Fig. 3 Geometry of PWRI in well-reservoir formation



$$\frac{\partial \phi(t)C}{\partial t} + \nabla(Cv) - \nabla^2(DC) = -(\sigma_n + R_d) + R_n \quad (1)$$

$$C = C(x, z, t); 0 \leq x \leq L; 0 \leq z \leq Z; t \geq 0 \quad (2)$$

$$C(x, z, 0) = C_0$$

$$C(L, z, t) = 0 \quad (3)$$

$$\left[\frac{\partial C}{\partial r} \right]_{(r=R, Z, t)} = 0 \quad \left[\frac{\partial C}{\partial z} \right]_{(x, Z=Z, t)} = 0 \quad (4)$$

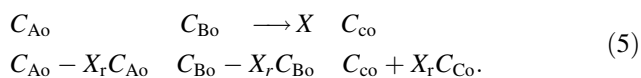
where C is the concentration of produced water active constituents, C_0 is the initial concentration of the active constituents, v is the produced water transport velocity in the geologic formation, $\phi(t)$ is the variable porosity, D is the molecular diffusivity, and t is time.

The significant control variables in improved PWRI model are as follows:

σ_n deposition filtration term, R_n geochemical reaction term, R_d adsorption kinetics term, DC molecular transport term.

In this work, the geochemical reaction rate mechanism was described to follow second-order kinetics summarized as Eqs. 5 and 7 as follows.

At time $t = 0$



At time $t = t$

$$C_A \quad C_B \quad C_C \quad (6)$$

1 mol of Component A reacted with 1 mol of Component B to produce 1 mol of scale products:

$$R_n = \frac{1}{V_{fm}} \frac{\partial C}{\partial t} = K_o \left(\frac{C_T}{1 + \sum K_i C_i} \right) (C_A C_B - K_1 C) \quad (7)$$

$$R_n = \frac{\partial R_m}{\partial t} = K_o \left(\frac{C_T}{1 + \sum K_i C_i} \right) (C_A C_B - K_1 C) \quad (8)$$

These important contributions in the improved model were used to standardize the general performance of produced water reinjection in hydrocarbon aquifers, with geochemical reaction, adsorption kinetics, and hydrodynamic dispersion transport that highlighted as the key performance indicators of the improved model, as illustrated in subsequent sections (see Fig. 4).

Invasion Zone Front 1

To account for adsorption kinetics (R_d) in internal filtration modeling, three linear adsorption isotherms which are Linear; Langmuir, and Freundlich isotherms were considered. Single particle (suspended) linear adsorption is shown in

$$C_s = K_a C \quad (9)$$

To determine the active mass transfer coefficient (K_a), the Arrhenius equation is introduced as follows:

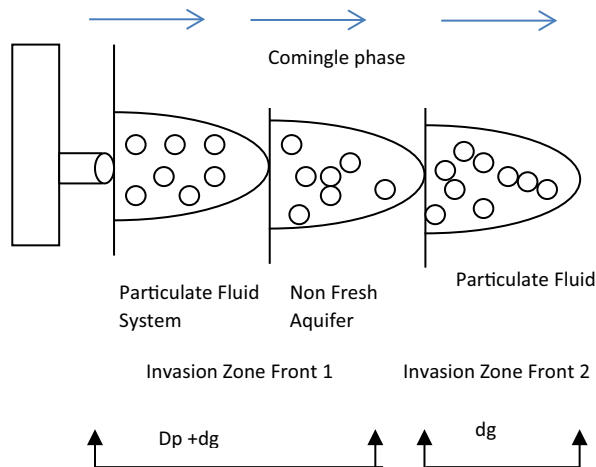


Fig. 4 Micro pore particle retention kinetics

$$K_a = K_o e^{-\frac{AH}{RT}} \quad (10)$$

The R_d macroscale adsorption particle retention kinetics (adsorption) on the surface of grain were computed and presented as Eq. 9:

$$\frac{\partial C_i}{\partial t} + \left(v_z \frac{\partial C_i}{\partial z} + \frac{v_\theta}{r} \frac{\partial C_i}{\partial \theta} + \frac{v_r}{r} \frac{\partial C_i}{\partial r} \right) - \left(D_z \frac{\partial^2 C_i}{\partial z^2} + D_r \left(\frac{\partial^2 C_i}{\partial r^2} + \frac{1}{r} \frac{\partial C_i}{\partial r} \right) \right) = R_d \quad (11)$$

With R_d is given by Eq. 12:

$$R_d = E_{mp} \left(\frac{1 - \phi_{mp}}{\phi_{mp}} \right) \left(\frac{3K_g}{R} \right) \left(C_i - \frac{C_T K_i C_i}{1 + \sum_{i=1}^n K_i C_i} \right) \quad (12)$$

where E_{mp} is defined as trapping efficiency factor. For particulate transport systems at the PW invasion zone when $t = 0$ and $0 < t < t_i$, where t_i is the residence time of the particle in invasion zone L_i . Previous studies illustrated that the suspended particles adsorbed have different dynamics in each invasion zone in the aquifer, thus the transport equation becomes

$$\left(\frac{\partial C_i}{\partial t} \right)_{L_i} + \left(E_{mp} \left(\frac{1 - \phi_{mp}}{\phi_{mp}} \right) \right)_{L_i} \left(\frac{\hat{k}k_g}{R} \left(C_T - \frac{C_T k_i c_i}{1 + \sum k_i c_i} \right) \right)_{L_i} = \left(-V_z \frac{\partial c_i}{\partial z} \right)_{L_i} + \left(-\frac{V_\theta}{r} \frac{\partial c_i}{\partial \theta} \right)_{L_i} + \left(-\frac{V_r}{r} \left(\frac{\partial}{\partial r} (rc_i) \right) \right)_{L_i} + \left(D_z \frac{\partial^2 c_i}{\partial z^2} \right)_{L_i} + \left(D_r \left(\frac{\partial^2 c_i}{\partial r^2} + \frac{1}{r} \frac{\partial c_i}{\partial r} \right) \right)_{L_i} \quad (13)$$

$$0 < L_i < L_{T_i}$$

The improved PWRI model in generalized dimensionless form accounts for residual oil mobility S_{or} and permeability k_{or} , porous media particle retention adsorption factor in Eq. 12:

$$\begin{aligned} & \left(\frac{\partial \zeta}{\partial \tau^*} - \left(\frac{\partial S}{\partial \tau^*} + \left(\frac{q_0}{c_0} \right) \frac{\partial \Psi_D}{\partial \tau^*} \right) + \left(\frac{R_0}{c_0} \right) \frac{\partial \Psi_r}{\partial \tau^*} \right) \\ & + \alpha_1(v) \left(\frac{\partial \zeta}{\partial \varepsilon_r} \right) + \alpha_2(v) \frac{\zeta}{\varepsilon_r} + \alpha_3(v) \frac{\partial \zeta}{\partial \varepsilon_z} \\ & = \alpha_4(v) \frac{\partial^2 \zeta}{\partial r^2} + \alpha_5(v) \left(\frac{\partial \zeta}{\partial \varepsilon_r} \right) + \alpha_6(v) \left(\frac{\partial^2 \zeta}{\partial \varepsilon_z^2} \right). \end{aligned} \quad (14)$$

Iwaski (1937) proposed the filtration model in Eq. 15 which represented the rate of particle trapping:

$$\frac{\partial \sigma}{\partial t} = \lambda v C \quad (15)$$

where v is the superficial velocity, λ is defined as the filtration coefficient, a function of a large number of parameters, and C is the fraction of suspended particles per unit volume of suspension.

The rate of deposition was proportional to the concentration of suspended particles and fluid velocity, see Eq. 14:

$$\frac{\partial \sigma}{\partial t} = \lambda \| U \| C_s. \quad (16)$$

The filtration coefficient was computed by the relation Eq. 17:

$$\lambda = \frac{3}{2} \left(\frac{1 - \phi}{d_s} \right) \alpha_c n \quad (17)$$

where α_c represents the total collision probability of the bed efficiency and n is the collision probability of the filtration mechanisms.

The Filtration Coefficient Numerical Model was computed as Eq. 16:

$$\begin{bmatrix} S_{i1} \\ S_{i2} \\ S_{i3} \\ \vdots \\ \vdots \\ S_{in} \end{bmatrix}_{K+1} = \begin{bmatrix} S_{i1} \\ S_{i2} \\ S_{i3} \\ \vdots \\ \vdots \\ S_{in} \end{bmatrix}_K + \alpha_0 \begin{bmatrix} \in_{i1} \\ \in_{i2} \\ \in_{i3} \\ \vdots \\ \vdots \\ \in_{in} \end{bmatrix}_K. \quad (18)$$

We assumed the following in the development of improved PWRI model:

- The displacing fluid (water) and the deposited solids were considered incompressible.
- The densities of the solid particles were considered equal in both dispersed and deposited states.
- The linear velocity in v_r , v_z , and v_ϕ along the core is constant. In addition, we assumed a constant velocity with time. Therefore, the conservation of the total flux is $d\omega v = 0$.
- The kinetics of the particles was considered linear.

- Dependency of the viscosity and concentration was considered negligible.
- Thermal and shear stresses were considered negligible.

The injectivity index was computed as flow rate per unit of the pressure drop between the injector and the reservoir and computed, see formula as shown in

$$\Pi = \frac{q(t)}{\Delta p(t)}. \quad (19)$$

The impedance was computed as the inverse of the dimensionless injectivity index:

$$J(T) = \frac{\Pi(0)}{\Pi(T)} = \frac{q_0 \Delta p(T)}{\Delta p(0) q(T)}. \quad (19)$$

The impedance was computed as piecewise linear function of the dimensionless time for either deep bed filtration or external cake formation (Pang and Sharma 1994, 1997; Prasad et al. 1999):

$$J_d(T) = 1 + mT \quad \text{For } T < T_r \quad (20)$$

$$J_d(T) = 1 + mT_r + m_c(T - T_r) \quad \text{For } T > T_r. \quad (21)$$

The nucleation or transition time T_r was represented as Eq. 22:

$$T_r > \frac{2\alpha r_w}{\lambda C_0 R_c^2}. \quad (22)$$

The impedance slope m during the deep filtration was computed by the formula of Eq. 22:

$$m_c = \frac{k k_{\text{rowr}} \varphi c_0}{k_c (1 - \varphi_c) X_w (-\ln X_w)} \quad (23)$$

$$\begin{aligned} m = & \left(\frac{\beta \varphi c_0}{\ln X_w} \right) (\lambda R_c) \left(\frac{1}{\sqrt{X_w}} \right) (-\exp(-\lambda(R_c - r_w)) \\ & - \lambda R_c \exp(\lambda r_w) \int_{\lambda r_w}^{\lambda R_c} \frac{\exp(-u)}{u} du \end{aligned} \quad (24)$$

where

$$u = \lambda R_c \sqrt{X} \quad (25)$$

$$X = \ell^2 = \left(\frac{r}{R_c} \right)^2 \quad (26)$$

$$X_w = \ell^2 = \left(\frac{r_w}{R_c} \right)^2. \quad (27)$$

m_c represent the slope of the external cake formation.

The damage section of the aquifer formation was computed as a ratio of differential in injection pressure over injection rate presented in Eq. 28:

$$\frac{\Delta P_\infty}{q} = \frac{\mu \ln \left(\frac{r_e}{r_w} \right)}{2\pi K_{or} K_\sigma}. \quad (28)$$

The undamaged section was computed as Eq. 29:

$$\frac{\Delta P}{q} = \frac{\mu \ln\left(\frac{r_e}{r_w}\right)}{2\pi K_{or}} \tag{29}$$

$$\begin{aligned} \text{Total Injectivity Pressure Gradient} &= \frac{\Delta P}{q} + \frac{\Delta P_{\infty}}{q} \\ &= (1 + K_{\sigma}) \frac{\mu \ln\left(\frac{r_e}{r_w}\right)}{2\pi h K_{or}} \end{aligned} \tag{30}$$

where

$$\frac{\Delta P_{\infty}}{q} = \frac{\mu \ln\left(\frac{r_e}{r_{ec}}\right)}{2\pi K_{or}} \tag{31}$$

$$\begin{aligned} \text{Total Impedance} &= \text{Damage Impedance} \\ &+ \text{Undamaged Impedance.} \end{aligned} \tag{32}$$

Figure 5 shows the damage section which represents area that has been affected by cake deposits, whereas undamaged section is unaffected by solids deposition.

The total impedance was computed by

$$\frac{\Delta P}{q} = \frac{\mu}{2\pi K_{or}} \left(\ln\left(\frac{r_e}{r_w}\right) + K'_{\sigma} \right). \tag{33}$$

The dimensionless form of total impedance index was computed as Eq. 33 as follows:

$$\frac{\left(\frac{\Delta P}{q}\right)_T}{\left(\frac{\Delta P_0}{q_0}\right)} = \frac{\left(\left(\ln\left(\frac{r_e}{r_w}\right) + K'_{\sigma}\right)\right)_T}{\left(\left(\ln\left(\frac{r_e}{r_w}\right)\right)_{\sigma}\right)_T} \tag{34}$$

where

$$j = 1 + K'_{\sigma} \left(\frac{1}{\ln\left(\frac{r_e}{r_w}\right)} \right). \tag{35}$$

The injectivity index was computed as the flow rate per unit of the pressure drop between the injector and the reservoir (Eq. 35):

$$\Pi = \frac{q(t)}{\Delta p(t)}. \tag{36}$$

Based on preliminary field data obtained from a field operator and regulator in Nigeria, the model was solved using finite-element method and the injectivity and solid deposition simulated in COMSOL environment. Details of

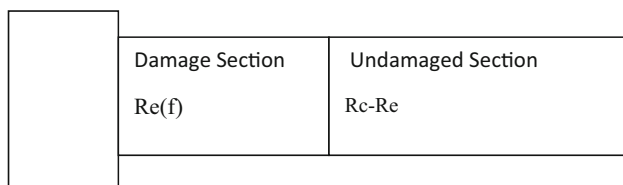


Fig. 5 Damage and undamaged section of a reservoir

the finite-element method and COMSOL software algorithms applied to solve the mode were presented in subsequent sections.

Field data, numerical development, and computer simulation

The improved PWRI model was solved by finite-element method and injectivity and permeability damage simulated in the COMSOL Multiphysics software environment using the field data obtained from regulator for the Onshore Field in Nigeria. In the numerical model, a six-order six-point implicit differencing scheme was used and resulting numerical solution of the governing equations of the PWRI concentration field was solved by the Triadiagonal Matrix Algorithm (TDMA) method. The implicit finite scheme was then applied to the PWRI Model of Eq. 5 to give Eq. 36:

$$\begin{aligned} \alpha'_1 \zeta_{ijk+1} + \alpha'_2 \zeta_{i+1jk+1} + \alpha'_3 \zeta_{ij+1k+1} + \alpha'_4 \zeta_{i-1jk+1} + \alpha'_5 \zeta_{ij-1,k+1} \\ = \alpha'_6 \zeta_{ijk} + \hat{a}_r \Delta q_{rijk} - \hat{a}_d \Delta q_{dijk} \end{aligned} \tag{37}$$

where

the adsorption term in Eq. (37) was specified by Eq. (38):

$$\begin{aligned} \Delta q_{dijk} &= \left(\frac{a_1}{\hat{a}_d}\right) \zeta_{ijk+1} - \left(1 - \frac{\hat{a}_2}{\hat{a}_d}\right) \zeta_{ijk} \\ &+ \left(1 - \frac{\hat{a}_2}{\hat{a}_d}\right) \left(C_T \frac{k_1}{1 + k_1 c_o \zeta_{ijk}}\right) \zeta_{ijk}. \end{aligned} \tag{38}$$

The other terms in Eq. (36) was defined in line with the reservoir:

$$\alpha'_1 = 1 - \Delta \tau^* \left(\frac{\alpha_1}{\Delta \epsilon_r} + \frac{\alpha_3}{\Delta \epsilon_z} - \frac{2\alpha_4}{(\Delta \epsilon_r)^2} - \frac{2\alpha_6}{(\Delta \epsilon_z)^2} \right) \tag{39}$$

$$\alpha'_2 = \left(\frac{\alpha_1 \Delta \tau^*}{\Delta \epsilon_r} - \frac{\alpha_4 \Delta \tau^*}{(\Delta \epsilon_r)^2} + \frac{\alpha_5 \Delta \tau^*}{\Delta \epsilon_r} \right) \tag{40}$$

$$\alpha'_3 = \left(\frac{\alpha_3 \Delta \tau^*}{\Delta \epsilon_z} - \frac{\alpha_6 \Delta \tau^*}{(\Delta \epsilon_z)^2} \right) \tag{41}$$

$$\alpha'_4 = \left(\frac{\alpha_4 \Delta \tau^*}{(\Delta \epsilon_r)^2} \right) \tag{42}$$

$$\alpha'_5 = \left(\frac{\alpha_6 \Delta \tau^*}{(\Delta \epsilon_z)^2} \right) \tag{43}$$

$$\alpha'_6 = 1 - \Delta \tau^* (\alpha_o + \alpha_2) \tag{44}$$

where

$$\alpha_1(v) = \left(\frac{v_r}{v}\right) \left(\frac{L}{R_o}\right) \tag{45}$$

Table 1 Re-injection parameters *source: Energy Tech Co, Houston, Texas, USA and petroleum regulator, Department of Petroleum Resources (DPR), as reported by (Idialu 2014)

Well	Perforations (md)	Tubing size	Inj. press.	Inj. rate	Inj start UP
A-5	12,173'-12,282'	4.5"	2505 psig	22 MBWPD	11/19/2000
A-10	15,060'-15,132'	5.5"	3342 psig	20 MBWPD	5/22/2001
A-12	17,152'-17,258'	5.5"	2504 psig	26 MBWPD	4/19/2001
A-14	26,772'-26,846'	5.5"	2359 psig	22 MBWPD	5/16/2003
A-19	20,990'-21,062'	5.5"	3240 psig	19 MBWPD	12/10/2001
Total Injection 109 MBWPD					

$$\alpha_2(v) = \left(\frac{v_r}{v}\right) \left(\frac{L}{R_o}\right) \left(\frac{1}{\epsilon_r}\right) \quad (46)$$

$$\alpha_3(v) = \frac{v_z}{v} \quad (47)$$

$$\alpha_4(v) = \left(\frac{D_{er}}{v}\right) \left(\frac{L}{R_o^2}\right) \quad (48)$$

$$\alpha_5(v) = \left(\frac{D_{er}}{v}\right) \left(\frac{L}{R_o^2}\right) \left(\frac{1}{\epsilon_r}\right) \quad (49)$$

$$\alpha_6(v) = \left(\frac{D_{ez}}{v}\right) \left(\frac{1}{L}\right). \quad (50)$$

Computation of Velocity in r and z direction:

$$v_r = \frac{q_r}{2\pi r h} = \left(\frac{K_{or} K_{\sigma_r}}{\mu}\right) \int_{r_w}^{r_{e1}} \frac{1}{r} \frac{drP}{dr} + \int_{r_{e1}}^{r_e} K_{or} \frac{1}{r} \frac{drP}{dr} \quad (51)$$

$$v_z = \frac{q_z}{\pi r^2 h} = \left(\frac{K_{oz} K_{\sigma_z}}{\mu}\right) \int_{r_w}^{r_{e1}} \frac{dP}{dz} + \int_{r_{e1}}^{r_e} K_{oz} \frac{dP}{dz} \quad (52)$$

$$\int_{r_w}^{r_e} \left(\frac{q}{2\pi h}\right) \frac{dr}{r} = \left(\frac{K_{or}(1+K_{\sigma_r})}{\mu}\right) \Delta P \quad (53)$$

$$\frac{\Delta P}{q} = \frac{\mu \ln\left(\frac{r_e}{r_w}\right)}{2\pi K_{or}} + \frac{\mu \ln\left(\frac{r_e}{r_w}\right)}{2\pi K_{or} K_{\sigma_r}} \quad (54)$$

$$\frac{\Delta P}{q} = \frac{1}{2\pi K_{or}} \left(1 + \frac{1}{K_{\sigma_r}}\right).$$

The flow chart in Fig. 4 described the simulation algorithm using the COMSOL Multiphysics software.

Field water compatibility studies for fields in Gulf of Guinea, Nigeria field in Niger Delta

The data of PWRI case studies for Gulf of Guinea (Niger Delta, Nigeria) were provided in operator's report planned for water flood for secondary enhanced recovery in the Niger Delta region of Nigeria. Five PWRI runs were assessed for this study. The limiting factors for injection rates were friction and pumping capabilities. Table 1

showed the data of field study conducted for PWRI programme in a field in Gulf of Mexico.

From these studies, friction contributed significant part in PWRI performance which varied significantly depending on rate and tubing size. In addition, a number of other estimates were determined over a range of the variables of Young's Modulus, Poisson's Ratio, injection water temperature, and the difference in pressure between the reservoir pressure and flowing bottom hole pressure that were ran (Fig. 6).

Impact of water quality on matrix injection

The WID (Water Injectivity Decline) simulator results presented in Figs. 7 and 8 outlined the significance of water quality on injection rates and pressure. The simulator was developed at the University of Texas. The output shows injectivity vs. time. The injectivity is dimensionless permeability, and the half-life is the amount of time, in days, at which the dimensionless permeability drops to half the original value. The output based on their results shown in Fig. 7 is for matrix injection with very good water quality (1 ppm of 1 micron sized particles). The results show futility of trying to inject below the fracture gradient since injection rate declines in the matter of a few days to a fraction of the original value. The permeability profile shows that the damage is shallow, even with good perm (200 md).

The field data runs reviewed showed that water quality has a significant impact on the half-life. With 5 ppm of 5 micron solids, the half-life is about a year for a 100' fracture. This meant that the fracture will continue to grow at about this rate every year, assuming that it is confined to a single zone (Tables 2, 3).

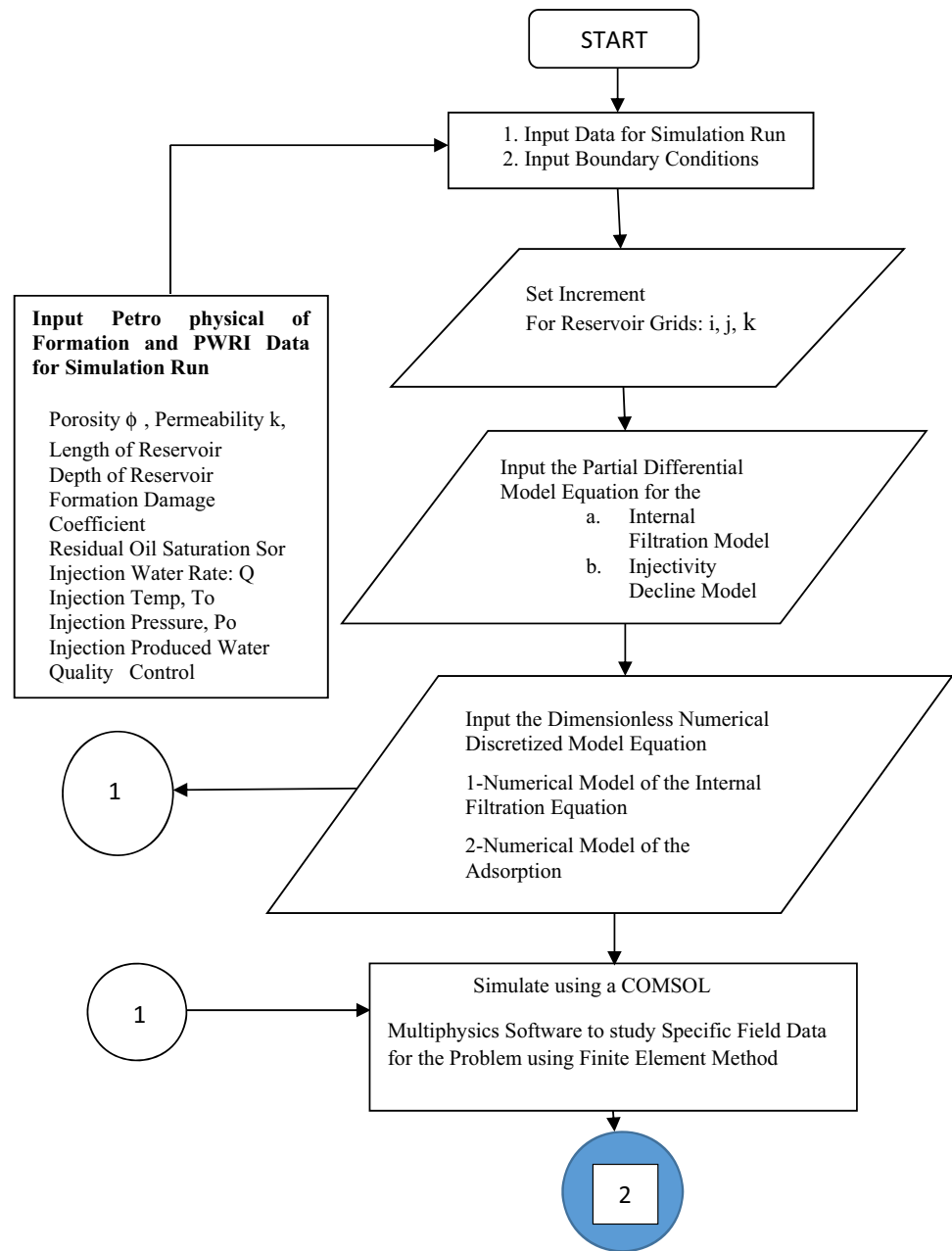
Results and discussions

The discussions of results of findings are presented as follows:

Injectivity profile with time

In this section, the results of injectivity with time are presented for two different studies obtained for two different

Fig. 6 Flow chart algorithm of simulation program for the PWRI model



fields, with the actual field data run compared with simulated data obtained from this work. Figure 9 results show plot of injectivity with time for a typical PWRI data obtained for a field in the Gulf of Mexico (Texas Fields) and were supplied by the field operator, while Fig. 10 shows the simulated injectivity based on data obtained from operator Nigerian Oil Field. While the numerical values of the simulated and field study may differ, injectivity profile trends obtained in Fig. 9 compared favorably with injectivity obtained in Fig. 10 simulated on the COMSOL Multiphysics platform thereby validating the improved PWRI model. The plots establish that injectivity decline

was spatially away from the produced water invasion zone in the host aquifer to settle at a threshold value. The transition time to cake formation for actual field run was 50 days while for our simulated run was observed to occur within 5 days. The blue line shown in Fig. 9 shows the injectivity decline for the field studies, while the grey line in Fig. 10 shows the injectivity decline profile simulated in COMSOL metaphysics environment where a correlation in trend was observed. The green line in Fig. 9 shows a steep change in injectivity near the well bore showing effect of geometry with respect to injection fracture with injection decline steepest at the well bore than further away.

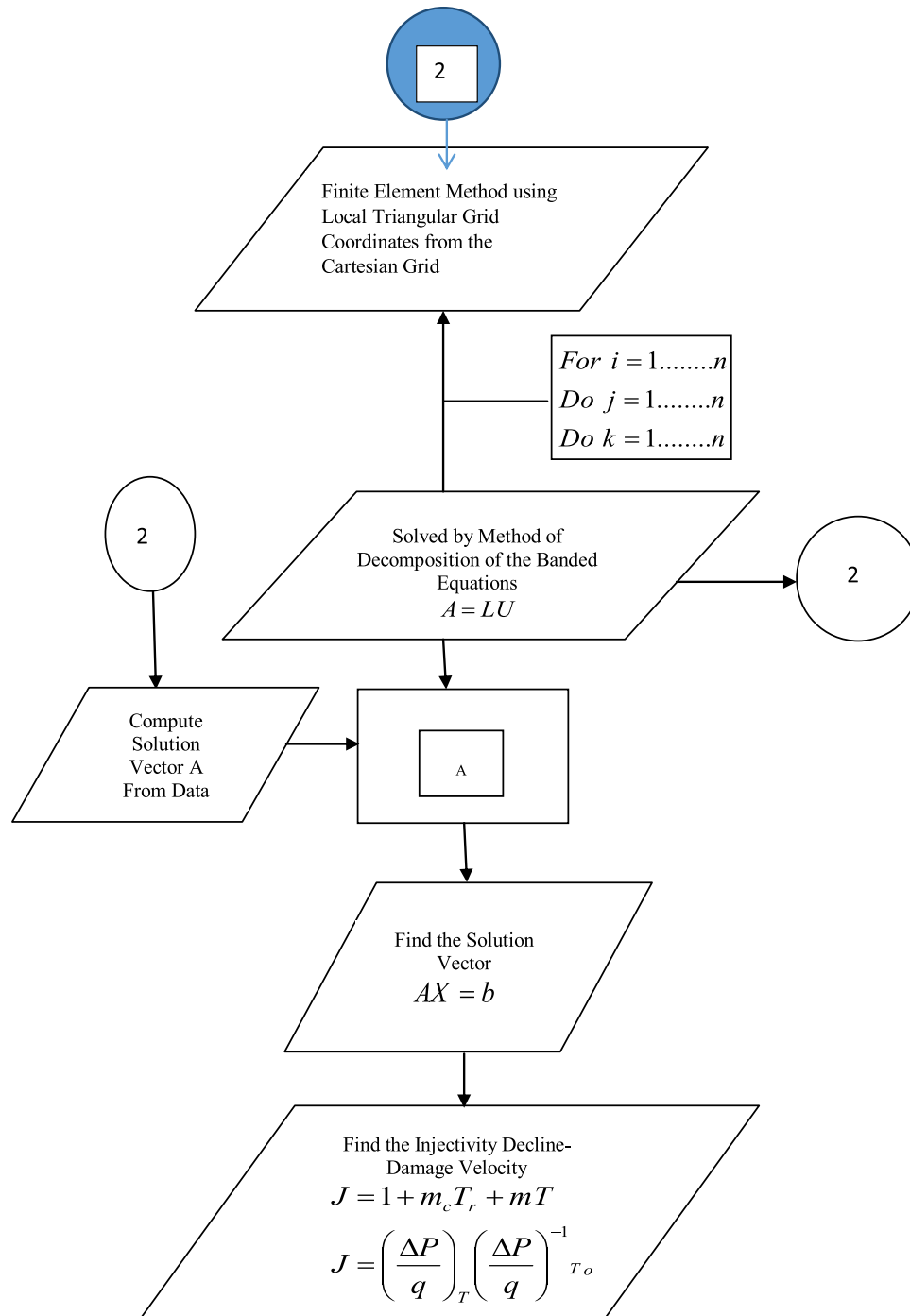


Fig. 6 continued

Effect of flow rate on injectivity with time

In this section, we show how higher injection rate and sweep volume could impact on injectivity decline and cake deposition. Figures 11 and 12 show the plots of the simulated injectivity decline against PWRI rates and

observed to be inversely proportional to each other. From plots increased injection rate led to decreased injectivity decline leading to sustained impairment and transition to cake formation which was minimized to a constant residual value. The sweep volume erodes deposition and adsorption on walls of aquifer, because drag force was

Fig. 7 1 ppm, 1 micron, Injectivity and perm profiles
*source: Energy Tech Co, Houston, Texas, USA and petroleum regulator, Department of Petroleum Resources (DPR), as reported by (Idialu 2014)

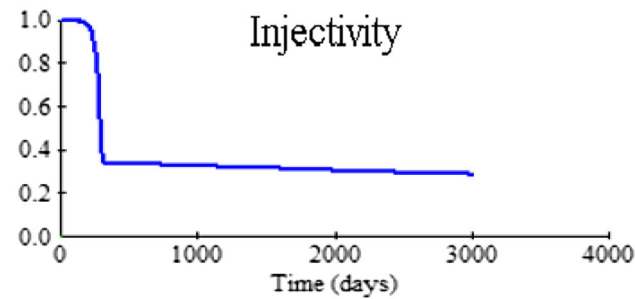
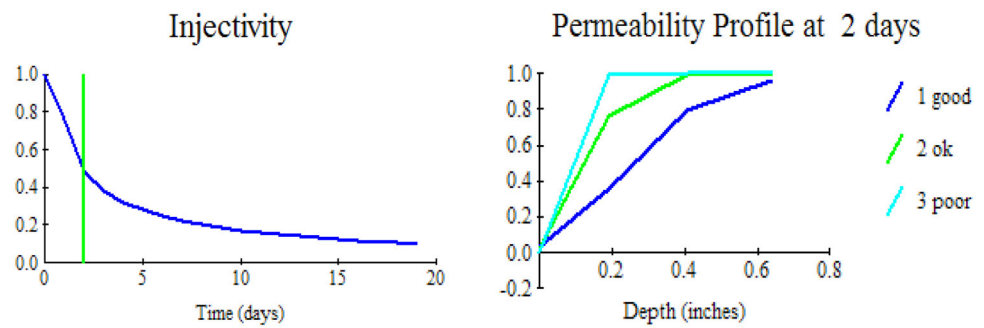


Fig. 8 60 md, 100 ft fracture, 5 ppm, 5 micron *source: Energy Tech Co, Houston, Texas, USA and petroleum regulator, Department of Petroleum Resources (DPR), as reported by (Idialu 2014)

observed to have the effect of reducing solids deposition to a constant injection rate. Previous studies showed that friction contributed significant role in PWRI performance and varied significantly depending on rate and tubing size.

Significant reduction in injectivity decline and fracturing could be attributed to larger drag force resulting from increased rates. These results were validated by Gulf of Mexico study presented in Table 1 where similar observations of plots of actual and simulated results trends were correlated. In addition, a number of other estimates over a range of the variables of Young’s Modulus, Poisson’s Ratio, injection water temperature, and the difference in pressure between the reservoir pressure and flowing bottom hole pressure were ran. The results in Fig. 11 showed futility of attempting to inject below the fracture gradient since injection rate declines in the matter of a few days to a fraction of the original value transient was followed by a steady state of constant injectivity beyond which decline remains constant after 15 days, transition time to cake formation irrespective of the injection rates. Injectivity decline increased as flow rate

Table 2 Sensitivity summary data *source: Energy Tech Co, Houston, Texas, USA and petroleum regulator, Department of Petroleum Resources (DPR), as reported by (Idialu 2014)

	Frac gradient	WHP	Young’s modulus	Poisson’s ratio	Injection temp	BHP–P _r injection	Friction
Best guess	0.60	2.545	2,500,000	0.1	80	2000	900
Highest pressure	0.70	4.603	2,000,000	0.08	150	2500	1500
Lowest pressure	0.49	1.134	3,000,000	0.125	60	1500	600
Best guess	0.60	2.545	2,500,000	0.1	80	2000	900
YM high	0.56	2.140	3,000,000	0.1	80	2000	900
YM low	0.64	2.950	2,000,000	0.1	80	2000	900
Best guess	0.60	2.545	2,500,000	0.1	80	2000	900
PR high	0.60	2.487	2,500,000	0.125	80	2000	900
PR low	0.60	2.589	2,500,000	0.08	80	2000	900
Best guess	0.60	2.545	2,500,000	0.1	80	2000	900
Temp high	0.68	3.379	2,500,000	0.1	150	2000	900
Temp low	0.57	2.307	2,500,000	0.1	60	2000	900
Best guess	0.60	2.545	2,500,000	0.1	80	2000	900
Press high	0.63	2.901	2,500,000	0.1	80	2500	900
Press low	0.56	2.190	2,500,000	0.1	80	1500	900
Best guess	0.60	2.545	2,500,000	0.1	80	2000	900
Friction high	0.60	3.145	2,500,000	0.1	80	2000	1500
Friction low	0.60	2.245	2,500,000	0.1	80	2000	600

decreases and vice versa. Formation around the fracture is impaired by deep penetration of solids, (ii) an external filter cake is built on the fracture wall by oil and solids

Table 3 WID run summary *source: Energy Tech Co, Houston, Texas, USA and petroleum regulator, Department of Petroleum Resources (DPR), as reported by (Idialu 2014)

Perm	Particle size, microns	Concentration, ppm	Half-life, days	Frac Length, ft
All three zones	1	1	2	0 (matrix injection)
200	5	5	152	50
200	2	2	381	50
200	1	1	766	50
60	5	5	298	100
60	5	5	155	50
60	2	2	385	50
60	1	1	770	50
5	2	2	403	50
5	1	1	790	50

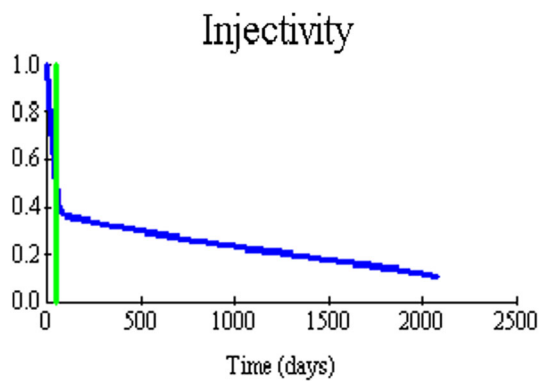
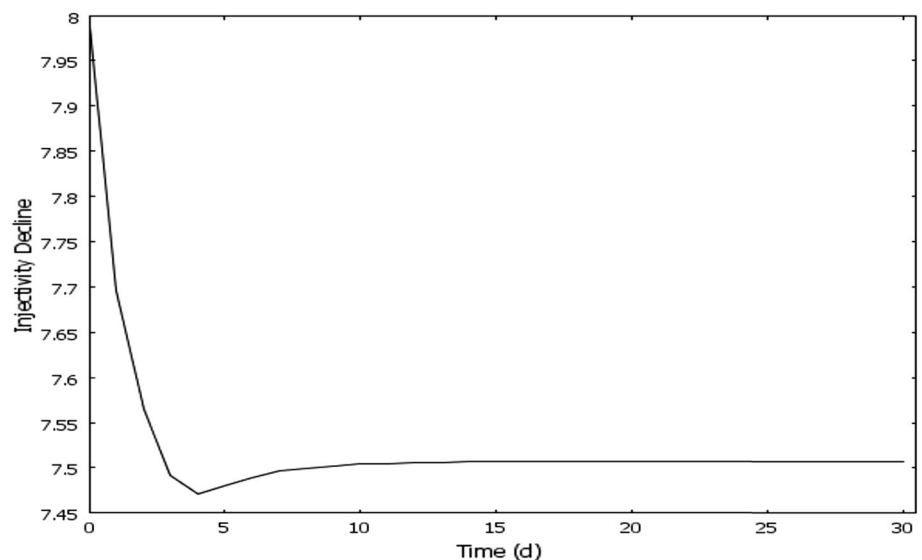


Fig. 9 Field studies, injectivity with time

Fig. 10 Injectivity profile with time (days)



that remain in the fracture and (iii) filter cake growth eventually leads to plugging of the fracture. The injectivity decline was dependent on injection rate impact on produced water invasion zone flooding volume in aquifer formation with a lower sweep volume leading to higher injectivity decline and in increase of the produced water sweep volume rate leads to higher injectivity performance and, therefore, higher recovery.

Effect of particle size and formation damage on injectivity

In this section, the effects of particle size on injectivity with time were studied and demonstrated. Figure 13 showed decrease in injectivity with time as the particle size decreases. The particle to grain size $\left(\frac{dp}{dg}\right)$ of 0.6164 showed lower injectivity decline than a particle to grain size $\left(\frac{dp}{dg}\right)$ of 0.2740. The smaller particles were able to penetrate the pores faster than larger grain particles in suspended solids thereby increasing chances for internal cake formation and external cake build up. The plots showed that injectivity index decreased from 1.135 to 1.1 in 30 days. The impact of particle to grain size is a function of adsorption capacity of particles on aquifer wall to form cake deposits significant in altering injectivity and formation damage alongside quality of constituents, injection rate of produced water which were established in the previous section.

Figure 14 outlined the variation of injectivity decline with velocity damage factor. The plots showed decreased injectivity as damage factor increased irrespective of time the produced water is transported in the reservoir. The damage factor is a numerical index of the reduction in permeability resulted from formation damage due to

Fig. 11 Effect of flow rate on injectivity

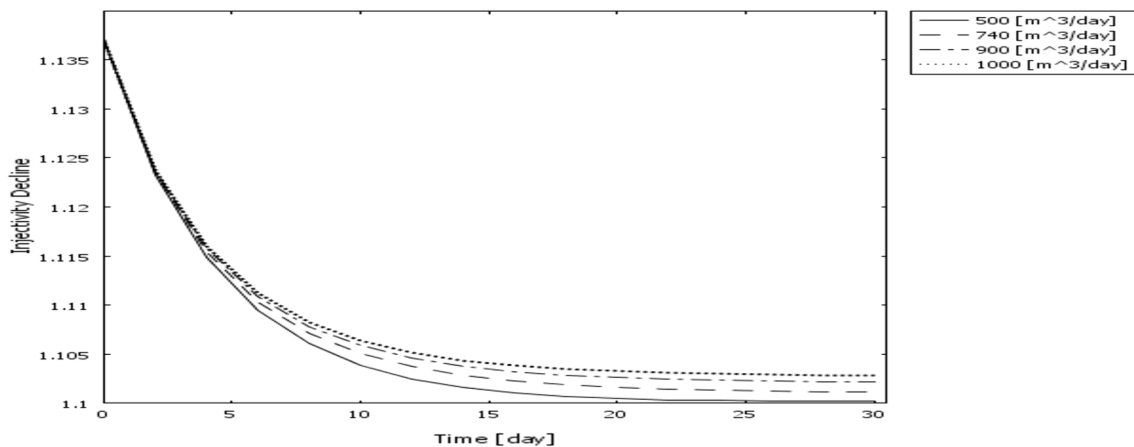
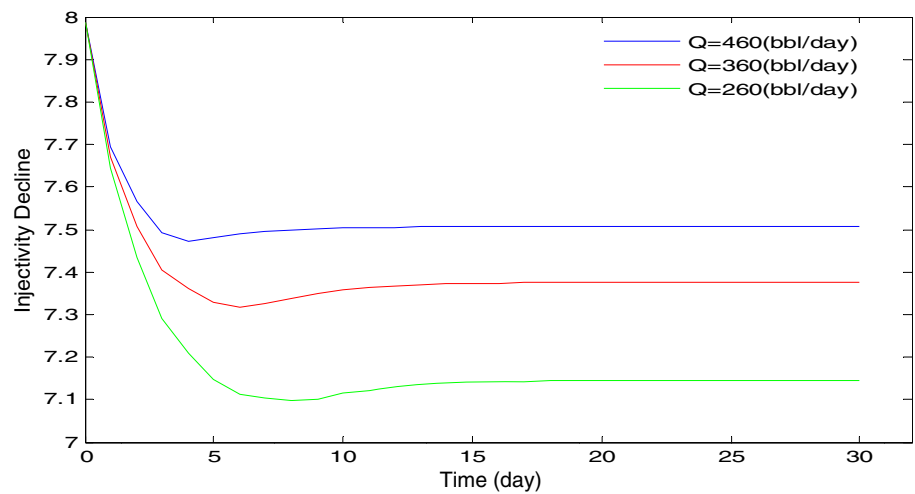


Fig. 12 Injectivity against time and flow rate. $\left(\frac{d_p}{d_g}\right)$ is the particle to grain ratio

scaling. However, the extent of decline of injectivity with damage factor was observed to invariant with time. The injectivity was same irrespective of the time for any specific damage factor.

Profile of permeability damage with distance

Figure 15 showed the profile of permeability on both fracturing and filtration phenomena. The profile decreased with time and increased uniformly with radial distance from produced water invasion zone. From the analysis of the results in the absence of particle deposition, low permeability formation were observed to be more likely fractured as the net fracturing pressure was observed to be inversely proportional to permeability, for a given injection rate. In addition, particle filtration and formation damage were governed by the interactions of particles in the injected water within the reservoir. In general, formation plugging is severe as the formation permeability decreased.

However, from results, formation permeability was directly dependent on the formation grain size (d_g). A comparison of the profile in Fig. 16 and the permeability of field data of Fig. 15 showed a good agreement for damage permeability, with a little allowance for lithological variation and other factors that may partially contribute to injectivity variation.

Effect of temperature variation on injectivity with time

Figure 17 outlines the significance of temperature variation as a key role in adsorption rate in the Arrhenius equation and subsequently injectivity decline. Higher temperature favors greater retention rates outlining the importance of adsorption rate in particle deposition. The fracture gradient was influenced as temperature changes which led to less injectivity as temperature increases. As cooler injection fluids reduce temperature, the rock becomes more brittle

Fig. 13 Effect of particle size on injectivity with time. dp/dg is the particle to grain ratio

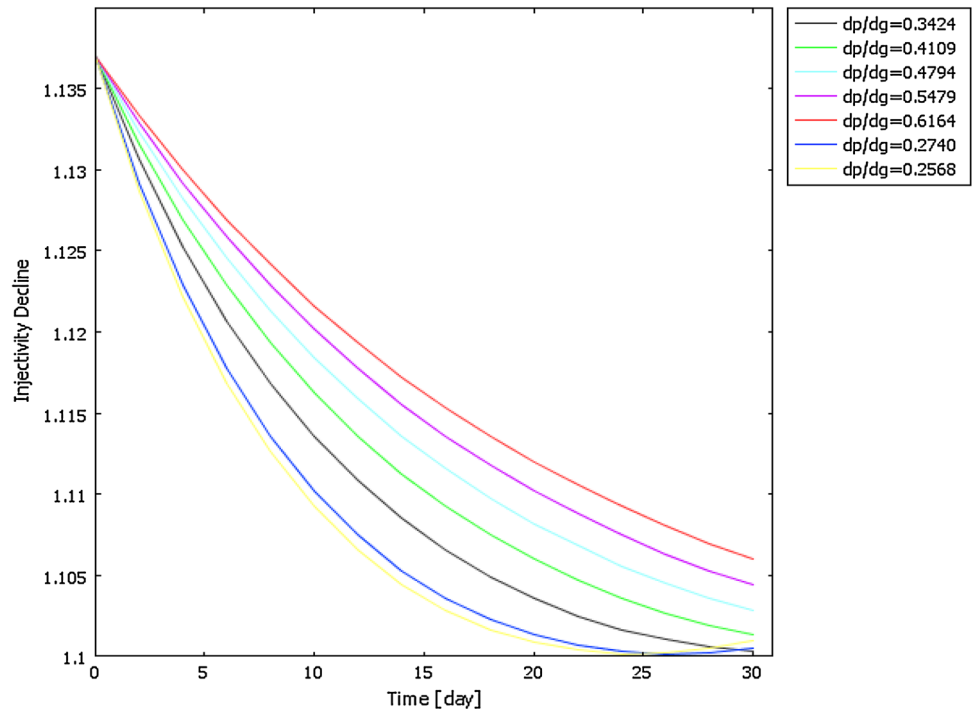


Fig. 14 Variation of injectivity decline with damage factor

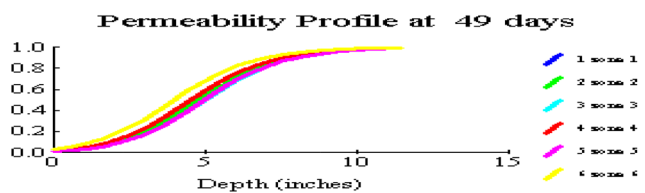
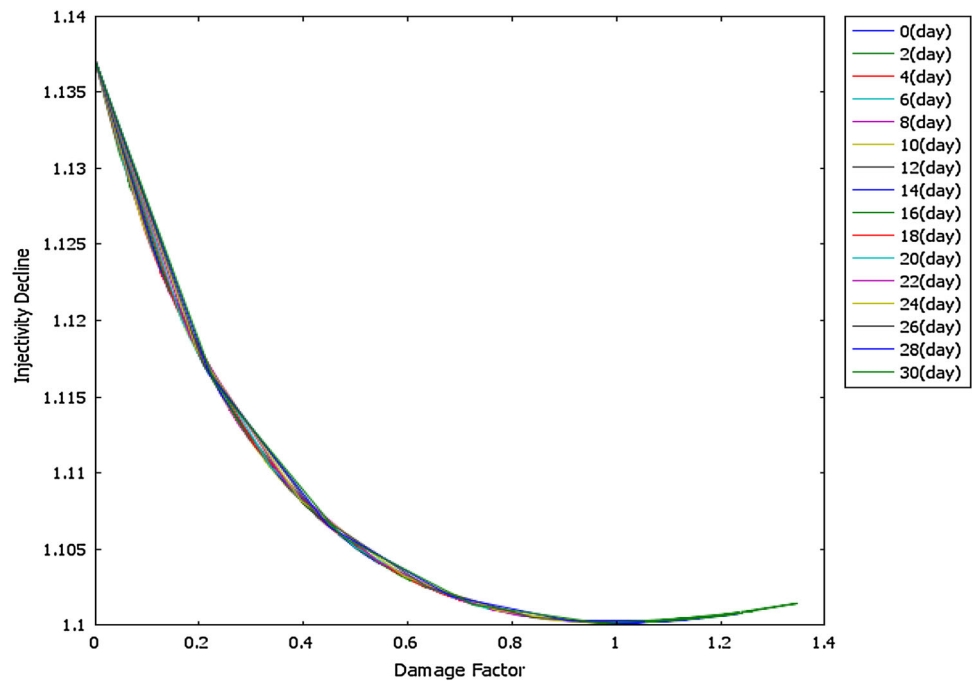


Fig. 15 Field simulation data of profile of permeability with depth at different zones

and this effect is strongly dependent on Young’s Modulus of elasticity. The profile is an exponential decrease in injectivity with time as temperature decreases.

Concentration variation with depth for first 5 days

Figure 18 showed the concentration of suspended and deposited solids decreases exponentially with depth. At an

Fig. 16 Profile of permeability damage with distance

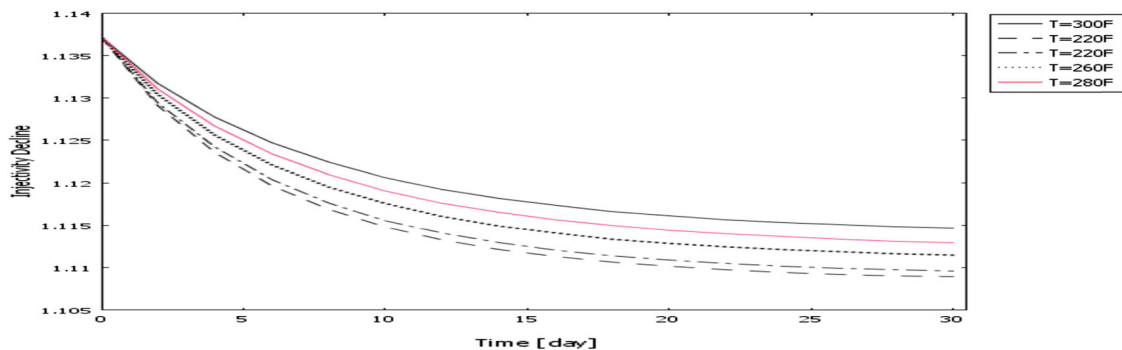
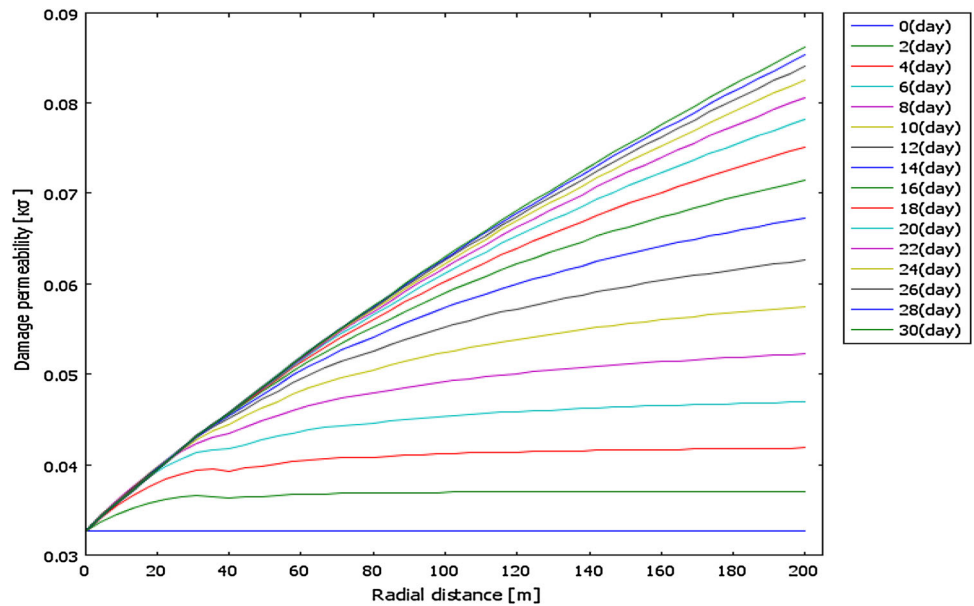
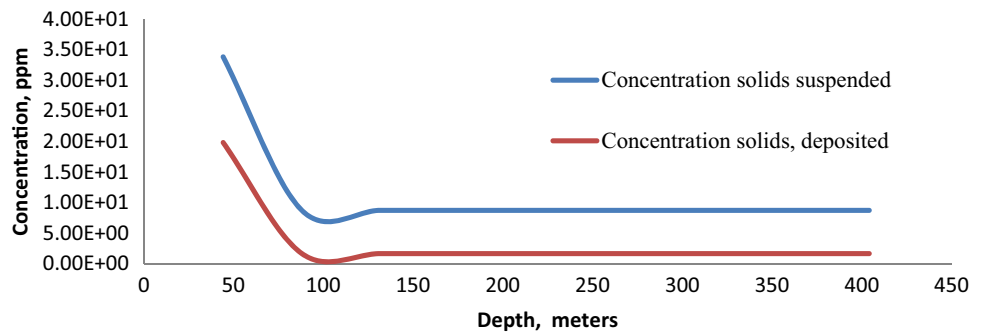


Fig. 17 Effect of temperature variation on injectivity with time

Fig. 18 Variation of concentration (suspended and deposited solids) with time for the first 5 days, of injection for calcite geochemical reaction index $SI = 1.48$



assumed depth 100 m, the concentration decrease reaches a minimum after which concentration remains constant. The effect of geochemical reaction scaling is apparent as concentration solids deposited was observed to be less than concentration in suspension.

Figure 19 outlines simulation of injectivity performance with time for the reservoir temperature temp = 164 °F and Flow Line temp = 125 °F for calcite

geochemical reaction which has a scaling index $SI = 1.48$. The significant results reveal Injectivity decline is exponential in time. For a water injection rate of 5000 bbls/day, injectivity decline is a maximum on the first day and remain constant for the remaining days as it progresses. The simulation results show potential calcite scaling of $SI = 1.48 > 1$ induces a faster time to injectivity decline.

Fig. 19 Profile of injectivity with time for reservoir temp = 164 °F and flow line temp = 125 °F for calcite geochemical reaction index SI = 1.48

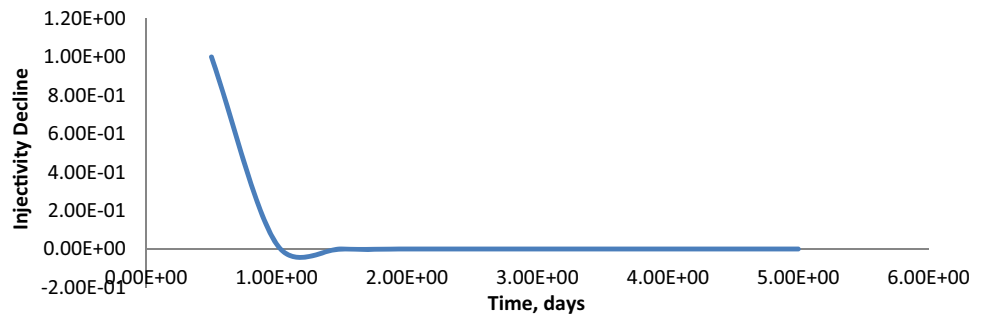


Fig. 20 Profile of Concentration (suspended and deposited) with radial distance at TVD 44.2 m and at 5 days Reservoir Temp = 164 °F and Flow Line Temp = 125 °F for Calcite Geochemical Rxn Index SI = 1.48

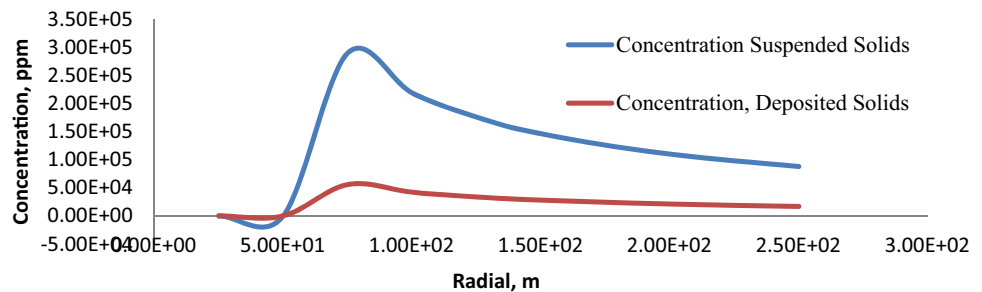


Figure 20 is the profile of concentration of suspended and deposited solids with radial distance on the 5th day for injection at 5000 bbl/day (TVD 44.2 m and time 1 day) for reservoir temp = 164 °F and flow line temp = 125 °F for Calcite Scaling Index SI = 1.48. Concentration decreases for deposited and suspended solids after 50–100 m may be the result of increased deposition precipitated due to increased geochemical scaling.

Conclusion

An improved PWRI model incorporating the effect of geochemical reaction, adsorption kinetics and hydrodynamics molecular transport was presented to predict performance of produced water reinjection Schemes in hydrocarbon aquifer. The model was solved using a finite-element method with the injectivity and solids deposition simulated in COMSOL Multiphysics Software. At a specific length in the aquifer, the concentration profile of the active specie follows an exponential distribution in time. Meanwhile, injectivity decline decreases exponentially with radial distance in the aquifer. The injectivity decline was found to be a function of cake deposition resulting from geochemical reaction, adsorption kinetics coupled filtration scheme and molecular diffusion. In conclusion, we established that the

transition time t_r to cake nucleation and growth was a consequence aquifer capacity, filtration coefficients particle and grain size diameters and, more importantly, adsorption kinetics, geochemical reaction and produced water quality.

Acknowledgements The support for this work by the Energy Tech Co, Houston Texas and Department of Petroleum Resources for supplying research data is greatly acknowledged. The support of systems engineering staff and technical and research assistant at the department of chemical engineering is acknowledged for their assistance in COMSOL multiphysics software programming of data and models.

Open Access This article is distributed under the terms of the Creative Commons Attribution 4.0 International License (<http://creativecommons.org/licenses/by/4.0/>), which permits unrestricted use, distribution, and reproduction in any medium, provided you give appropriate credit to the original author(s) and the source, provide a link to the Creative Commons license, and indicate if changes were made.

Appendix A: field validation simulation on nigerian onshore field

The field data for the study was supplied by the operator of the onshore field (Field X) in Nigeria Licensed by the Regulator is presented below (Tables 4, 5).

Table 4 Reservoir/well data of sample of study area

Sample name	Units	FieldX-10ST	Field X-12HST	Field X-13HST	Field X-18ST	Field X-26	Field X produced water
Data sampled							20/3/08
Analysis		VRMT	VRMT		VRMT	VRMT	VRMT
Field		X	X		X	X	Produced Water
Well		10	12	13	18	26	
Reservoir		R-03/X-02	R-03/X-05	R-03/X-06	R-17/X-06	R-03/X-06	
Interval (TVD)	(ft)	8709-10164	7702-9385	7310-8510	7282-7340	5891-5890	
Datum	(ft)	6026	5898	5897	7296	5880	
Initial reservoir pressure	Psia	2457	2571	2546	2913	2534	n/a
Initial reservoir temperature	°F	164	163	162	188.75	162	n/a
Flow line pressure	Psia	105	120	125	450	125	n/a
Flow line temperature	°F	124	122	119	128	120	n/a
Average gas production	MScf/d	1309	1433	510	778	294	n/a
Average oil production	bbl/day	1740	2600	1623	1501	940	n/a
Average water production	bbl/day	2.0	2.7	405	0.5	1.0	n/a

Table 5 Produced water parameters quality

Parameters	Symbol	FieldX-10ST	Field X-12HST	Field X-13HST	Field X-18ST	Field X-26	Field X produced water
pH							
Density	g/cc	8.37	8.64	8.40	8.41	8.43	7.95
Total dissolved solid	mg/l	15,050.00	9640.00	12,720.00	14,720.00	12,680.00	16,000.00
Chloride	mg/l	9996.9	6797.89	9447.07	9597.02	8797.27	10946.00
Sulphate	mg/l	124.55	80.68	104.82	130.80	94.22	39.12
Total alkalinity	mg/l	900.00	560.00	1633.33	833.33	833.33	1520
Sodium	mg/l	7251.72	4996.41	6163.06	7410.69	6188.79	2773.02
Potassium	mg/l	198.75	148.56	213.51	221.80	179.96	104.10
Calcium	mg/l	43.50	46.40	64.60	51.60	106.00	303.25
Magnesium	mg/l	27.50	25.60	37.80	36.00	26.00	51.12
Strontium	mg/l	0.20	0.24	0.33	0.36	26.00	51.12
Barium	mg/l	1.55	1.76	2.01	2.12	1.48	1.32
Iron	mg/l	0.84	0.13	0.03	0.31	0.21	0.86
Carbonate	mg/l	240	96	320	80	160	0.00
Bicarbonate	mg/l	610	488	1342	854	692.33	1854
Phosphate	mg/l	4.55	3.84	8.68	2.96	1.80	
Hydroxide	mg/l	0.00	0.00	0.00	0.00	0.00	0.00
Copper	mg/l	0.07	0.00	0.12	0.84	0.36	
Nickel	mg/l	0.14	0.10	0.17	0.12	0.04	
Lead	mg/l	0.00	0.00	0.00	0.00	0.00	0.00
Zinc	mg/l	0.28	0.11	0.03	0.03	0.07	2.37
Quality control							
Total dissolved solids-calculated	mg/l	17,966	12,362	16,730	17,891	15,751	13,418.00
SP Gravity-calculated	g/cc	1.012	1.009	1.012	1.012	1.011	1.007

Table 6 Produced water injectivity quality

Well(s)	X10ST					Inhibitor	pH after precipitation
	Temp.	Press.	Calcite				
°F	Psia	pH	SI	ΔSI	mg/L	mg/L	
124	105	8.50	1.48	0.63	104	0.35	8.45
128	366	8.08	1.12	0.27	98	0.05	8.03
133	628	7.93	0.99	0.14	95	0.00	7.88
137	889	7.85	0.92	0.07	93	0.00	7.81
142	1,150	7.80	0.88	0.03	91	0.00	7.76
146	1412	7.77	0.86	0.01	90	0.00	7.73
151	1673	7.75	0.85	0.00	90	0.00	7.71
155	1934	7.74	0.85	0.00	90	0.00	7.70
160	2196	7.74	0.85	0.00	90	0.00	7.69
164	2457	7.73	0.85	0.00	90	0.00	7.69

Produced water analysis data

The water analysis data conducted at a Laboratory in Lagos is presented in the Table 6. The chemical indicators for QA/QC, such as Na/K, Ca/Mg, Ca/Na and TDS, are within ranges typical of formation waters. Several software programs have been used to calculate the scaling potential. The program ScaleSoftpitzer by Mason Thompson's Brine Consortia Group at Rice University reported used for all scaling tendency calculations. The program was designed for the prediction, treatment and control of common scale deposits in Oil and Gas wells. Scale SoftPitzer quantitatively calculates the scaling potential up the wellbores. It used the formation water compositions, CO₂ and H₂S content of the gas compositions or pH and the production rate data if available. The scaling potential is expressed in terms of saturation indices (SI) for scale minerals and the amount of scale deposits per volume of water in mg/l.

Saturation Index (SI) is defined as log of saturation ratio as shown below

$$SI = \text{Log}((\text{CaCO}_3)/K_{sp}) \quad (55)$$

K_{sp} is the solubility product of calcium carbonate.

Please note:

If $SI \leq 0$ No Scale formation should be expected.

If $SI \geq 0$ There is potential for Scale Formation

Field X-10ST

Self scaling Assessment-Calcite

Without commingling with field X produced water, Well X-10RST shows the tendency to form calcite scale at production conditions.

The field for study was based on data for an onshore field in Nigeria overseen by the Petroleum Regulator and National Oil Company. Without Commingling with Field

X produced water, Well X-10RST shows the tendency to form calcite scale at production conditions.

Model field study computer simulation analysis

The classical model developed for PWRI was solved by finite-element method in COMSOL multiphysics software environment using the field data presented above for an onshore field in Nigeria. The produced water from the Field X is planned for water flood for enhanced hydrocarbon recovery. Five produced water samples were collected for this study. The samples were from FieldX10st, Field X12st, FieldX13st, FieldX14st and Field X14t. Their corresponding reservoirs are R-03/X-02, R-03/X-05, R-03/X06, R17/X-06 and R-03/X-06, respectively. Water compatibility can be assessed by conducting the scaling tendencies predictions with respect to calcium carbonate (calcite) and barium Sulphate (Barite) of Field X produced water with formation water.

Appendix B: The field data used for simulation is presented below

Data

The chemical indicators for QA/QC such as Na/K, Ca/Mg, Ca/Na and TDS are within ranges typical of formation waters.

1) WELL 10 2) RESERVOIR B-03/X-02 3) INTERVAL (TVD) 8709-10164FT C

4) DATUM 6026 FT C 5) INITIAL RESERVOIR PRESSURE: 2457PSIA

6) INITIAL RESERVOIR TEMPERATURE: 164 °C FLOWLINE PRESSURE 105PSIA

OPEN (6, FILE = 'X.RES') 1) Initial Concentration of Deposits CD (1, 1, 1) = 0.0, 2) Time = 10 days 3)

Adsorption Constant Term $KAD = 3.0 \text{ mol/dm}^3 \text{ s}$ **3)** Total Length of Reservoir $RN = 500 \text{ m}$ **4)** Mole Constant $RG = 8.3149 \text{ kJ/kmol K}$ **4)** Pressure Gradient $DP = 0.000005 \text{ psia}$ **5)** Length of Damage Zone of Reservoir $RC = 200 \text{ m}$ **6)** Density of Particulate = 25 ppm **7)** Length of Well Bore $RW = 0.2 \text{ m}$ **8)** Water Injection Rate $Q = 5000 \text{ bbls/day}$ **9)** Initial Concentration of Suspended Particulate $CO = 25$ **10)** Permeability Damage Constant $BDAMG = 50$ **11)** Absolute Permeability $KABS = 501 \text{ m Darcy}$ **12)** Relative Permeability of Water in Formation $KROW = 0.5$ **13)** Relative Permeability if Water–Oil $KWOR = 0.5$ **14)** DATUM Height TVD of formation = 6026 ft **15)** Total Vertical Depth $TVD1 = 8709 \text{ ft}$ **16)** Total Vertical Depth $TVD2 = 10164 \text{ ft}$ **17)** The Heat of Activation $DHEA = 2.3 \text{ J/K}$ **18)** Filtration Coefficient $LAND = 20/\text{m}$ **19)** $VISC = 0.7 \text{ cp}$ **20)** Temperature of Formation $TEMPF = 164 \text{ }^\circ\text{F}$ **21)** Temperature of Reservoir $TEMPR = 124 \text{ }^\circ\text{F}$ **22)** Flow Rate of Gas in Formation $QGAS = 1309 \text{ MSfc/days}$ **23)** Flow Rate of Water in Formation $QWATER = 2.0 \text{ bbls/days}$ **24)** Flow Rate of Oil in Formation $QOIL = 1740 \text{ bbls/days}$ **25)** Heat of Reaction Constant $L1 = 0.06345 \text{ kJ/Kmol K}$ **26)** Temperature Conversion to $^\circ\text{F}$ **27)** $FTEMP = (5.0/9.0) * (TEMPF - 32)$ **28)** $RTEMP = (5.0/9.0) * (TEMPR - 32)$ **29)** $DTEMP = RTEMP - FTEMP$ **30)** $TEMPD = DTEMP / \text{LOG}(RTEMP/FTEMP)$ **31)** $KG = L1 * \text{EXP}(-DHEA / RG * TEMPD)$ **32)** Grant Sites concentration $CT = 1.0$ **33)** Porosity of Reservoir, $P_{or} = 0.22$ (33) Porosity of Cake, $P_{orc} = 0.12$

Produced water re-injection data used in COMSOL multiphysics software Simulation

Variable	Values
c_d	0
k	$2e-3$
r_w	0.2
K_{or}	0.5
K_{abs}	$50e-15$
K_Q	50
r_e	10
R_g	8.314
C_T	1
ρ	25
DH	2.3
T	346.483
C_o	25
Q	1360
v_{is}	0.0007
A_o	$2e20$
k_1	$A_o * \text{exp}(-DH / (R_g * T))$

Appendix continued

Variable	Values
l_a	20
E_n	200
E_{np}	300
r_c	200
DP	$\text{vis} * \log(r_c/r_w) / (2 * \pi * K_{or} * K_Q)$
d	443.484
v_r	$(DP * K_{abs} * K_{or} * K_Q) / (v_{is} * \log(r_c/r_w) * r_e * d)$
P_o	0.22
tan	$\text{tan}(P_o)$
n	$3 / P_o * (1 / \text{tan} - 1 / P_o)$
A	$\pi * d^2 / 4$
u	Q / A
D	0.2
f_g	0.023
r_d	$d / 2$
v	$Q / (2 * \pi * r_d * 200)$
B	50
alpha	0.1
R_c	200
T_r	$(2 * \alpha * r_w) / (l_a * C_o * R_c^2)$
X_w	$(r_w / R_c)^2$
RAmi	$n * ((1 - P_o) / P_o) * \rho * q_t$
r_2	$(1 - P_o) / P_o * (3 * f_g / R_g)$
r_3	$C - (CT * k_1 * C) / (1 + k_1 * C)$
RAma	$r_2 * r_3$
R_d	RAmi + RAma
K_c	$1 / (1 + B * C)$
K_{c1}	$1 / K_c$
$r_c r_w$	$1 / (\log(r_c/r_w))$
J	$1 + K_{c1} * r_c r_w$
DP ₃	$(Q * \text{vis}) / (2 * \pi * K_{or}) * (\log(r_c/r_w) + K_{c1})$
IJ	1/J
vr ₁	$(DP_3 * K_{abs} * K_{or} * K_Q) / (\text{vis} * \log(r_c/r_w) * r_e * d)$
Q_n	$l_a * vr_1 * C$
R	$-(Q_n + R_d)$

References

Abou-Sayed AS, Zaki KS, Wang GG, Sarfare MD (2005) A mechanistic model for formation damage and fracture propagation during water injection. In: Paper 94606 presented at the SPE European formation damage conference, Sheveningen

Abou-Sayed AS, Zaki KS, Wang GG, Sarfare MD, Harris MH (2007) produced water management strategy and water injection best practices: design, performance and monitoring. SPEPO 22(1):59–68

Ajay S, Sharman MM (2007) A model for water injection into frac-packed wells. In: Paper SPE 110084 presented at the 2007 annual technical conference, Anaheim CA

- Al-Abduwani FAH (2005) Internal filtration and external filter cake build-up in sandstones. PhD Dissertation, Delft University of Technology, Delft. ISBN 90-9020245-5
- Al-Abduwani FAH, van den Broek WMGT, Currie PK (2001) Visual observation of produced water re-injection under laboratory conditions. In: Paper 68977 presented at the SPE European formation damage conference, The Hague
- Altoef JE, Bedrikovetsky P, Gomes ACA, Siqueira AG, Desouza AI (2004) Effects of oil water mobility on injectivity impairment due to suspended solids. In: SPE Asia Pacific oil and gas conference
- Barkman JH, Davidson DH (1972) Measuring water quality and predicting well impairment. *J Petrol Technol* 24:865–873
- Bedrikovetsky P, Marchesin D, Shecaira F, Souza AL, Milanez PV, Resende E (2001) Characterization of deep bed filtration system from laboratory pressure drop measurements. *J Petrol Sci Eng* 32:167–177
- Bedrikovetsky P, Furtado CA, de Souza ALS, Siquera FD (2007) Internal erosion in rocks during produced and sea water injection. In: SPE paper 107513 presented at the SPE Europe/EAGE annual conference and exhibition held in London, UK
- Chang CK (1985) Water quality considerations in Malaysia's first water flood. In: *JPT*, September, pp 1689–1698
- Clifford PJ, Mellor DW, Jones TJ (1991) Water quality requirements for fractured injection wells. In: SPE 21439, presented at the SPE middle east oil show, November, pp 851–862
- Davidson DH (1979) Invasion and impairment of formation by particulates. In: Paper 8210, presented at the SPE annual technical conference and exhibition, Las Vegas
- De Zwart AH (2007) Investigation of clogging processes in unconsolidated aquifers near water supply wells. PhD Dissertation, Delft University of Technology, Delft
- Dong CY, Wu L, Wang AP (2010) Experimental simulation of gravel-packing in horizontal and highly deviated well. *J China Univ Petrol* 34(2):74–82
- Donaldson EC et al (1977) Particle transport in sandstones. In: Paper SPE 6905, presented at the 1977 SPE, annual technical conference and exhibition, Denver, Colorado
- Doresa R, Hussaina A, Katebaha M, Adhama S (2012) Advanced water treatment technologies for produced water. In: Proceedings of the 3rd international gas processing symposium
- Farajzadeh R (2002) Produced water re-injection (PWRI)—An experimental investigation into internal filtration and external cake buildup. MSc. Thesis, Delft University of Technology, Delft
- Faruk C (2010) Non-isothermal permeability impairment by fines migration and deposition in porous media including dispersive transport. *Transp Porous Media* 85:233–258
- Folarin F, An D, Caffrey S, Soh J, Sensen CW, Voordouw J, Jack T, Voordouw G (2013) Contribution of make-up water to the microbial community in an oilfield from which oil is produced by produced water re-injection. *Int Biodeterior Biodegradation* 81:44–50
- Furtado CJA, Siquera AG, Souza ALS, Correa ACF, Mendes RA (2005) Produced water reinjection in petrobas fields: challenges and perspectives. In: Paper 94705 presented at the SPE Latin American and caribbean petroleum engineering conference, Rio de Janeiro, Brazil
- Gong B, Liang H, Xin Z, Li K (2013) Numerical studies on power generation from co-produced geothermal resources in oil fields and change in reservoir temperature. *Renew Energy* 50:722–731
- Greenhill K (2002) Brazil frade fluid properties technical service report. In: EPTC TS02000099, November 15
- Guedes RG, Al-Abdouwani FA, Bedrikovetsky, Currie PK (2006) Injectivity decline under multiple particle capture mechanisms. In: Paper 98623 presented at SPE internal symposium and exhibition on formation damage control, Lafayette
- Hustedt B, Zwartz D, Bjoerndal HP, Mastry R, van den Hoek PJ (2006) Induced fracturing in reservoir simulation: application of a new coupled simulator to water flooding field examples. In: Paper 102467 presented at spe annual technical conference and exhibition held in San Antonio, Texas, USA
- Idialu PO (2014) Modeling of adsorption kinetics, hydrodynamic dispersion and geochemical reaction of produced water reinjection (PWRI) in hydrocarbon aquifer. PhD Thesis, Department of System Engineering, University of Lagos
- Iwaski T (1937) Some notes on sand filtration. *J Am Water Works Assoc* 29:1591
- Khatib Z (2007) Produced water management: is it a future legacy or a business opportunity for field development. In: International petroleum technology conference (IPTC 11624), held in Dubai, UAE
- Khodaverdian M, Sorop T, Postif S, van den Hoek PJ (2009) Polymer flooding in unconsolidated sand formations: fracturing and geochemical considerations. In: Paper 121840 presented at the SPE Europe/EAGE annual conference and exhibition held in Amsterdam
- Lawal AK, Vesovic V (2010) Modeling Asphaltene-induced formation damage in closed systems. In: SPE Paper 138497 presented in international petroleum exhibition and conference, Abu Dhabi
- Lawal KA, Vesovic V, Edo SB (2011) Modeling permeability impairment in porous media due to asphaltene deposition under dynamic conditions. *Energy Fuels* 25:5647–5659
- Li M, Li Y, Wang L (2011) Productivity prediction for gravel-packed horizontal well considering variable mass flow in wellbore. *J China Univ Petrol* 35(3):89–92
- Li Y, Li M, Qin G, Wu J, Wang W (2012) Numerical simulation study on gravel-packing layer damage by integration of innovative experimental observations. In: Paper 157927 presented in SPE Heavy Oil Conference held in Calgary, Alberta
- Mendez ZDC (1999) Flow of dilute oil-in water emulsions in porous media, PhD, the University of Texas
- Nabzar L, Chaveteau G, Roque C (1997) A new model for formation damage by particle retention. In: Paper 31119 presented at the SPE International symposium on formation damage control, Lafayette, USA, pp 14–15
- Ochi J, Detienne J-L, Rivet P (2007) Internal formation damage properties and oil deposition profile. *Soc Petrol Eng*. doi:10.2118/108010-MS
- Ojukwu KI, van den Hoek PJ (2004) A new way to diagnose injectivity decline during fractured water injection by modifying conventional hall analysis. In: Paper 89376 presented at the SPE/DOE 14th symposium on improved oil recovery held in Tulsa, Oklahoma, USA
- Pang S, Sharma MM (1994) A model for predicting injectivity decline in water injection wells. In: Paper SPE 28489 presented at the 1994 annual technical conference, New Orleans
- Pang S, Sharma MM (1997) A model for predicting injectivity decline in water injection wells. *SPE Form Eval* 12(3):194–201
- Prasad KS, Bryant SL, Sharma MM (1999) Role of fracture face and formation plugging in injection well fracturing and injectivity decline. In: Paper 52731 presented at the 1999 SPE/EPA conference held in Austin, Texas
- Sahni A, Kovacevich ST (2007) Produced water management alternatives for offshore environmental stewardship. In: Paper 108893 presented at the SPE Asia Pacific health, safety, security and environment conference and exhibition held in Bangkok, Thailand
- Salehi MR, Settari A (2008) Velocity-based formation damage characterization method for produced water re-injection: application on masila block core flood tests. University of Calgary, Alberta
- Sharma MM, Pang S, Wennberg KE, Morgenthaler LN (2000) Injectivity decline in water-injection wells: an offshore Gulf of



- Mexico case study. In: SPE production and facilities, February, pp 6–13
- Shuler PJ, Subcaskey WJ (1997) Literature review: oily produced water reinjection. CPTC TM97000078 in March
- Souza ALS, Figueiredo MW, Kuchpil C, Bezerra MC, Siquera AG, Furtado C (2005) Water management in petrobras: developments and challenges. In: Paper OTC 17258 presented at the offshore technology conference, Houston, Texas, USA
- Todd A (1979) Review of permeability damage studies and related North Sea water injection. In: Presented at the society of petroleum engineers international symposium on oilfield and geothermal chemistry, Dallas
- Van den Hoek PJ, Matsuura T., Dekroon M, Gheissary G (1996) Simulation of produced water re-injection under fracturing conditions. In: Paper 36846 presented at the SPE European petroleum conference held in Milan, Italy
- Wang YF, Le TT (2008) Experimental study on the relationship between sand particle migration and permeability in unconsolidated sandstone reservoirs. *J Oil Gas Tech* 30(3):111–114
- Wang LY, Gaa CX, Mbadinga SM, Zhou L, Liu JF, Gu JD, Mua BZ (2011) Characterization of an alkane-degrading methanogenic enrichment culture from production water of an oil reservoir after 274 days of incubation. *Int Biodeterior Biodegradation* 65:444–450
- Wennberg KE, Sharma MM (1997) Determination of filtration coefficient and transition time for water injection wells. In: Paper 38181 presented at SPE European formation damage conference, The Hague
- Yerramilli RC, Zitha PLJ, Yerramilli SS, P (2013) A novel water injectivity model and experimental validation using CT scanned core-floods. In: Paper 165194, presented at the SPE European formation damage conference and exhibition held in Noorwijk
- Zeinjahromi A, Lemon P, Bedrikovetsky P (2011) Effects of induced fines migration on water cut during water flooding. *J Petrol Sci Eng* 78:609–617
- Zhang NS, Somerville JM, Todd AC (1993) An experimental investigation of the formation damage caused by produced oily water injection. In: Paper 26702 presented at the offshore Europe, Aberdeen